Jack Wilkie*, Georg Rauter, and Knut Möller

Initial engagement and axial force model for self-tapping bone screws.

https://doi.org/10.1515/cdbme-2022-1192

Abstract: Correctly torquing bone screws is important for implant fixation longevity and strength. A model-based smart screwdriver has been proposed to regulate torque, however current models ignore axial force and the initial engagement of the screw. This was addressed here by deriving a model based on the concept of a net axial force generated by a difference in contact areas on the inward and outward sides of the screw threads. This force is opposed by the shear strength of the material around the threads. The results of the derivation were able to predict the effects of different axial forces during insertion in relation to the hole material strength. The results may be used to compensate for initial thread breakage in future model-based smart screwdrivers to improve their accuracy.

Keywords: Bone screw, smart screwdriver, parameter identification, axial force, screw engagement.

1 Introduction

Bone screws are used in many orthopaedic procedures to secure implants and facilitate healing. These fixations must be strong and long-lasting for optimal patient outcomes. Correct torquing is an important factor affecting these criteria. Overtighting may damage threads cut in the bone, reducing fixation strength, while under-tightening may result in loosening, reducing longevity.

In current clinical use, screws are usually tightened by hand using tactile feel and experience. While surgeons are skilled, this is a subjective method that may be affected by factors like stress and fatigue. Hence, a more objective method of torque regulation may be desirable.

An automated model-based torque-regulation system has been proposed [1]. This requires a model of screw insertion to identify bone strength from torque and displacement signals, and another model to predict the optimal torque from this strength. Current work has focused on development [1–4], simulation [1], and experimental testing [4, 5]. Alternative empirical approaches include using a multiple of the screw's steady-state torque [6], detection of a spike in the torque derivative [7], or monitoring acoustic emissions [8].

The current work in model-based torque regulation focuses on torque as a function of angular displacement. Two factors that have not yet been considered are the initial engagement of the screw in the hole and the effects of axial force on the insertion. This paper will attempt to model these factors and produce some useful insights based on the model. The intention is for this model to later be integrated into the above-mentioned insertion models to improve overall performance of the torque-regulation system.

2 Methods

2.1 Model Derivation

The principle behind the model derivation is that as the screw thread cuts into the hole walls, the hole material is displaced plastically, and provides a normal reaction stress on the contacting area of the thread approximately equal to the compressive strength of the material. This normal reaction force pushes on the screw in the axial direction. For the purposes of this analysis, we assume the stress of the thread surface is always the ultimate compressive strength, σ_{ucs}, but this assumption will be discussed while interpreting the results. 'Up' is the direction away from the hole, and 'down' is towards it. The angular position of the screw, ϕ, is the screw rotation after the tip of the thread first begins to cut into the side of the hole; ϕ' represents a helical co-ordinate axis on the screw, measuring from the first contact point. Further parameters are explained in Tab. 1.

The triangular thread has upper and lower halves. The forces on the upper half push the screw down into the hole, and the forces on the lower half push the screw up out of the hole. As the lower half reaches the hole first, there is always more area of the lower half in contact than the upper half ($\phi > 0$). Given the assumed constant stress, the forces from the lower thread exceed those of the upper thread, giving a net upwards force. To simplify the complex mechanics here, we simply take the net force, and assume it is evenly distributed as shear stress over the screw envelope in the hole material. The screw envelope is roughly equivalent to a convex hull of

***Corresponding author: Jack Wilkie,** ITeM, HS-Furtwangen, VS-Schwenningen, DE, e-mail: wij@hs-furtwangen.de
Georg Rauter, BIROMED-Lab, University of Basel, Basel, CH
Knut Möller, ITeM, HS-Furtwangen, VS-Schwenningen, DE

Tab. 1: Parameters used in evaluation.

Symbol	Value	Unit	Name
D_h (r_0)	3.2	mm	Hole diameter
D_s (r_1)	6.5	mm	Screw major diameter
α	2π	rad	Angular length of thread cutting section of screw.
p	2.75	mm	Screw thread pitch
μ	0.17		Hole-screw friction co-efficient
θ_t	60	degrees	Screw end taper
L	25	mm	Screw threaded length
σ_{ucs}	4	MPa	Hole material strength

the screw geometry; we approximate the envelope with a 'Helical Cylinder' as shown in Fig. 1.

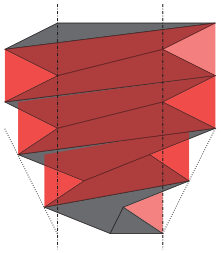

Fig. 1: Illustration of screw envelope. Red areas denote the "Helical Cylinder" shape that the shear force is assumed to be evenly distributed over. Dashed lines denote the edges of the hole, and dotted lines denote the taper.

The thread areas at the edge of the hole are demonstrated in Fig. 2. The lower thread extends helically past the point where the tip of the thread exits the hole, with the outer diameter of the contact area reducing to equal the inner diameter over a half turn. This gives an additional area, B_2 after the tip of the thread exits the hole. The upper thread reduces to nothing before the tip of the thread exits the hole, with the inner diameter of the area increasing up to the outer diameter over a half turn, so the upper thread area is reduced by A_1 before the thread tip exits the hole. These areas are also plotted in a rectangular projection in Fig. 3.

Considering the case of the screw initially entering the hole, shown in Fig. 3, the outer diameter of the screw thread will not have reached its full diameter. This also means that the hole surface effects described above will be scaled as shown in Fig. 3, and the ramp of inner/outer diameters will occur over $\pi(\phi/\alpha)$ rad instead of a half turn.

To calculate the total areas, the MATLAB R2020a symbolic toolbox integration was used. The general cases ($\phi > \alpha$) from Fig. 3 were implemented as a sum of 3 double integrals, and the special cases for initial engagement ($\phi < \alpha$) were the sum of two double integrals. The integration limits were

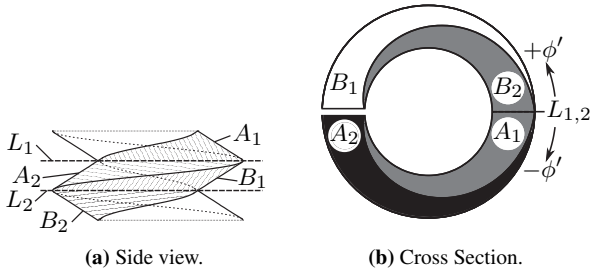

(a) Side view. **(b)** Cross Section.

Fig. 2: Relevant areas of upper and lower thread contact. L_1 is the surface level (tip of thread at surface) separating the areas in contact (A_2) or not (A_1) for the upper thread. Likewise L_2 is the surface level separating the area in contact (B_2) or not (B_1) for the lower thread. L_1 and L_2 are are coincident in (**b**), with $+\phi'$ going above and $-\phi'$ going below the surface. White indicates neither side in contact, grey is for only the lower thread, and black is both sides.

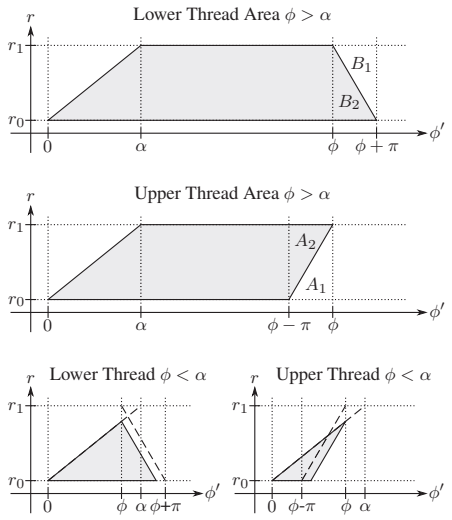

Fig. 3: Plot of thread contact areas. A_1, A_2, B_1, and B_2 are the same as in Fig. 2. Showing general case after initial engagement ($\phi > \alpha$), and special case while the thread cutting section is relevant ($\phi < \alpha$).

set based on the r and ϕ' values shown in Fig. 3, including appropriate considerations for slopes. The integrand to find the relevant cross-section thread area was $rcos(\theta_{\text{helix}})drd\phi'$, where θ_{helix} is the thread helix angle calculated as $\theta_{\text{helix}} = \arctan\left(\frac{p}{2\pi r_1}\right)$. As the difference in areas is the most important to find the net force, this was then calculated by subtracting the top area from the bottom, then multiplied by σ_{ucs} to give the net force. The net force equations were then output from MATLAB with the simplify() then latex() functions, and are shown in equations 1 and 2.

$$F_{\text{GENERAL}} = \frac{2\,\sigma_{\text{ucs}}\,\pi^2\,\left(-2\,{r_0}^2 + r_0\,r_1 + {r_1}^2\right)}{3\,\sqrt{\frac{p^2+4\,\pi^2\,{r_1}^2}{{r_1}^2}}} \tag{1}$$

$$F_{\text{SPECIAL}} = -\frac{\phi\,\sigma_{\text{ucs}}\,\pi^2\,(r_0 - r_1)\left(\begin{array}{l}3\,\alpha^2\,r_0 + 3\,\alpha^2\,r_1 - 2\,\phi^2\,r_0 \ldots \\ +2\,\phi^2\,r_1 + 3\,\alpha\,\phi\,r_0 - 3\,\alpha\,\phi\,r_1\end{array}\right)}{3\,\alpha^3\,\sqrt{\frac{p^2+4\,\pi^2\,{r_1}^2}{{r_1}^2}}} \tag{2}$$

The net force was distributed over the screw envelope shown previously in Fig. 1. The average radius of the currently inserted part was derived, giving eqn. 3. Then the area was calculated in eqn. 4 by considering the hole surface area currently above the edge of the thread, but under the material surface; the radius was factored out of this calculation. The radius and area were both piecewise functions, transitioning at α and 2π radians, respectively. For simplicity in this analysis, α has been kept at 2π giving the overall eqn. 5. The average shear force was calculated by simply dividing the net force by the envelope surface area.

$$r = \begin{cases} r_0 - \frac{\phi\,(r_0 - r_1)}{2\,\alpha} & \text{if } \phi < \alpha \\ r_0 + (r_0 - r_1)\left(\frac{\alpha}{2\,\phi} - 1\right) & \text{if } \alpha \leq \phi \end{cases} \tag{3}$$

$$\frac{A}{r} = \begin{cases} \frac{p\,\phi^2}{4\,\pi} & \text{if } \phi < 2\,\pi \\ p\,(\phi - \pi) & \text{if } 2\,\pi \leq \phi \end{cases} \tag{4}$$

$$A = \begin{cases} \frac{p\,\phi^2\left(r_0 - \frac{\phi\,(r_0 - r_1)}{4\,\pi}\right)}{4\,\pi} & \text{if } \phi < 2\,\pi \\ p\,(\phi - \pi)\left(r_0 + (r_0 - r_1)\left(\frac{\pi}{\phi} - 1\right)\right) & \text{if } 2\,\pi \leq \phi \end{cases} \tag{5}$$

2.2 Model Application

The equations developed in the previous section were evaluated using the parameter values in Table 1. The net force and average shear stress values were plotted for 0.01-20π radians. The equivalent shear stress was calculated according to the von Mises failure criterion [9], and was plotted horizontally over the shear stress; the angular displacement point where the shear stress equalled the failure stress was also plotted vertically.

For comparison, a screw with these parameters was inserted into 3 polyurethane (PU) foam blocks with 20N axial force. Photos were taken of the holes after removal.

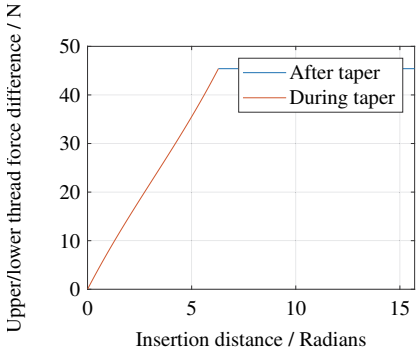

Fig. 4: Difference between forces on upper and lower thread assuming σ_{ucs} over both surfaces. Using parameters from Table 1.

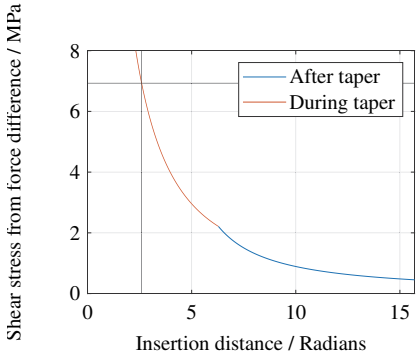

Fig. 5: Average shear force on surface of screw envelope in hole. Black lines indicate where stress equals the material strength.

3 Results

Fig. 4 shows the difference between the total force on the inward-facing/lower part of the thread profile, and the force on the outward-facing/upper part of the thread profile. This can be interpreted as the net force pushing the screw out of the hole from normal forces on the screw thread. It can also be interpreted as the required force (as a function of insertion angle) to counteract this outward net force and prevent breakage of the newly-formed threads. The figure shows that the force difference linearly increases from 0 N to 45.1 N between 0 rad and 2π rad; thereafter the force difference remains constant at 45.1 N.

Fig. 5 shows the average shear stress on the surface of the screw envelope. It also shows the point where the stress first falls below the shear strength of the material (2.60 radians).

Fig. 6 shows several holes in PU foam blocks of different strengths after screw insertion and removal with 20 N axial force. The holes in the 0.4 and 10 MPa materials show more damage around the entry point than the 4 MPa material.

(a) 0.8 MPa **(b)** 4 MPa **(c)** 10 MPa

Fig. 6: Condition of holes in 3 PU foam blocks with different compressive strengths after screw insertion with 20N axial force.

4 Discussion

For optimising screw insertion torque and improving parameter ID accuracy, there are two main points from these results.

Firstly, the axial insertion force should counteract the net forces like those plotted in Fig. 4. This requires a continuously adjusted force. Alternatively a constant force at the midpoint could be used. The net force in Fig. 4 is based on 4 MPa material strength; so a force around the 20N midpoint should be ideal for this material. This is supported by Fig. 6, where the 4 MPa material with a 20 N axial force showed the least thread damage; the axial force is too high for the 0.8 MPa material and compresses the material around the entry, while it is too low for the 10 MPa material, so the outward net force shears off the initial threads.

Secondly, if these axial forces are not counteracted, then the newly formed threads would start to break until the shear stress on the screw envelope became low enough. This is demonstrated in Fig. 5. As the broken threads would contribute less to the friction torque on the screw, which is part of the main mechanism for detecting strength from insertion torque [3], this would lower the insertion torque, which would normally lead to a lower estimated material strength. With the model developed here, it should be possible to compensate for this during the parameter identification.

The modelling process has a few limitations. Assuming the shear stress is evenly distributed over the screw envelope will give a lower maximum shear than for a more accurate non-uniformly distribution. Additionally, the screw envelope shape is a simple approximation, and could be modelled with a more detailed curved shape. For simplicity, the screw thread was assumed to be triangular with the minor diameter matching the hole diameter; while bone screws have complex curved thread profiles; extending the model similarly to Wilkie et al. [3] may be advantageous. Lastly, the model does not consider the dynamic effects of thread breakage on the net force and screw envelope area; while modelling these effects may be complex, it may provide valuable insights.

5 Conclusion

A model screw initial engagement developed, considering the imbalanced forces on the screw from differing areas of thread on the upper and lower parts of the thread profile. This model gave axial force recommendations consistent with experimental results. This should allow for these factors to be compensated for in an automatic torque-regulating screwdriver to achieve better accuracy and improve patient outcomes.

Assumptions regarding screw envelope, stress distribution, and thread shape may be improved upon in the future.

Author Statement

Research funding: Partial support by grants “CiD” and “Digitalisation in the OR” from BMBF (Project numbers 13FH5E02IA and 13FH5I05IA). Conflict of interest: Authors state no conflict of interest. Ethical approval: The conducted research is not related to either human or animal use.

References

[1] J. Wilkie, P. D. Docherty, and K. Möller, “Model-based bone material property identification,” *at - Automatisierungstechnik*, vol. 68, pp. 913–921, Nov. 2020.

[2] J. Wilkie, P. D. Docherty, and K. Möller, “Developments in Modelling Bone Screwing,” *Current Directions in Biomedical Engineering*, vol. 6, pp. 111–114, Sept. 2020.

[3] J. Wilkie, P. D. Docherty, T. Stieglitz, and K. Möller, “Geometric Generalization of Self Tapping Screw Insertion Model,” in *2021 43rd Annual International Conference of the IEEE Engineering in Medicine Biology Society (EMBC)*, pp. 4387–4339, Nov. 2021.

[4] J. Wilkie, P. D. Docherty, and K. Möller, “Stripping Torque Model for Bone Screws,” *IFAC-PapersOnLine*, vol. 54, pp. 442–447, Jan. 2021.

[5] J. Wilkie, P. D. Docherty, T. Stieglitz, and K. Möller, “Quantifying Accuracy of Self-Tapping Screw Models,” in *2021 43rd Annual International Conference of the IEEE Engineering in Medicine Biology Society (EMBC)*, pp. 4391–4394, Nov. 2021.

[6] K. J. Reynolds, A. A. Mohtar, T. M. Cleek, M. K. Ryan, and T. C. Hearn, “Automated Bone Screw Tightening to Adaptive Levels of Stripping Torque,” *Journal of Orthopaedic Trauma*, vol. 31, pp. 321–325, June 2017.

[7] R. L. Thomas, K. Bouazza-Marouf, and G. J. S. Taylor, “Automated surgical screwdriver: Automated screw placement,” *Proc Inst Mech Eng H*, vol. 222, pp. 817–827, May 2008.

[8] B. J. Wright, S. Grigg, A. S. Bergsaker, J. E. Brattgjerd, H. Steen, and R. Pullin, “Real time monitoring of screw insertion using acoustic emission can predict screw stripping in human cancellous bone,” *Clinical Biomechanics*, vol. 76, p. 105026, June 2020.

[9] R. von Mises, “Mechanik der festen Körper im plastisch-deformablen Zustand,” *Nachrichten von der Gesellschaft der Wissenschaften zu Göttingen, Mathematisch-Physikalische Klasse*, vol. 1913, pp. 582–592, 1913.